Targeting CXCL12/CXCR4 signaling with oncolytic virotherapy disrupts tumor vasculature and inhibits breast cancer metastases

Margaret Gil[a], Mukund Seshadri[b], Marcin P. Komorowski[a], Scott I. Abrams[a], and Danuta Kozbor[a,1]

[a]Department of Immunology and [b]Department of Pharmacology and Therapeutics, Roswell Park Cancer Institute, Buffalo, NY 14263

Edited by Kenneth I. Berns, University of Florida College of Medicine, Gainesville, FL, and approved February 20, 2013 (received for review November 27, 2012)

Oncolytic viruses hold promise for the treatment of cancer, but their interaction with the tumor microenvironment needs to be elucidated for optimal tumor cell killing. Because the CXCR4 receptor for the stromal cell-derived factor-1 (SDF-1/CXCL12) chemokine is one of the key stimuli involved in signaling interactions between tumor cells and their stromal microenvironment, we used oncolytic virotherapy with a CXCR4 antagonist to target the CXCL12/CXCR4 signaling axis in a triple-negative 4T1 breast carcinoma in syngeneic mice. We show here that CXCR4 antagonist expression from an oncolytic vaccinia virus delivered intravenously to mice with orthotopic tumors attains higher intratumoral concentration than its soluble counterpart and exhibits increased efficacy over that mediated by oncolysis alone. A systemic delivery of the armed virus after resection of the primary tumor was efficacious in inhibiting the development of spontaneous metastasis and increased overall tumor-free survival. Inhibition of tumor growth with the armed virus was associated with destruction of tumor vasculature, reductions in expression of CXCL12 and VEGF, and decrease in intratumoral numbers of bone marrow-derived endothelial and myeloid cells. These changes led to induction of antitumor antibody responses and resistance to tumor rechallenge. Engineering an oncolytic virus armed with a CXCR4 antagonist represents an innovative strategy that targets multiple elements within the tumor microenvironment. As such, this approach could have a significant therapeutic impact against primary and metastatic breast cancer.

viral oncotherapy | vascular targeting

The chemokine receptor CXCR4 and its cognate ligand CXCL12 form a pivotal axis for enabling metastasis by many solid tumor types, including breast carcinomas (1). Overexpression of CXCR4 in primary breast tumors is related to an aggressive phenotype and lymph-node metastases (2–4). Similarly, elevated CXCR4 expression in estrogen (ER) and progestin receptor (PR)-negative breast cancers, as well as $ER2^-/PR2^-/HER\text{-}2^-$ triple-negative breast cancers, is closely associated with lymph-node metastasis and poor prognosis (5, 6). Binding of CXCL12 to CXCR4 promotes tumor progression by several mechanisms associated with the activation of a number of signaling pathways required for biological responses, including chemotaxis (7). First, CXCR4 is essential for metastatic spread to organs where CXCL12 is expressed (8, 9). Second, CXCL12 can stimulate survival and growth of neoplastic cells in a paracrine fashion (10–12), and promotes tumor angiogenesis by recruiting circulating endothelial progenitor cells (CEPs) to the tumor stroma (10, 13). CXCL12 also attracts protumor $Gr1^+CD11b^+$ myeloid cells and regulatory T cells ($CD4^+$ subtype) into the tumor (14, 15), which impede innate and adaptive immune mechanisms of tumor destruction.

In contrast to normal breast tissue, breast cancer cells typically express high levels of CXCR4 that can direct chemotaxis and invasive responses (1, 4). Therefore, modulation of the CXCL12/CXCR4 signaling pathway in breast cancer could impact multiple aspects of tumor progression. Several CXCR4 antagonists have shown antitumor activity in preclinical models and have been evaluated in clinical trials (8, 16, 17). However, given the abundant expression of CXCR4 by many cell types, including those of the central nervous, gastrointestinal, and immune systems (18), the side-effects of these antagonists need to be considered. Moreover, the impact of soluble CXCR4 antagonists on the mobilization of CXCR4-expressing hematopoietic stem and progenitor cells represents an additional concern, particularly when combined with chemotherapeutic agents, because of the potential for increased toxicity to the normal process of hematopoiesis (8, 19).

To overcome some of these concerns related to the systemic delivery of soluble CXCR4 antagonists, we designed a tumor cell-targeted therapy that delivered the CXCR4 antagonist via an oncolytic vaccinia virus (OVV). To that end, a new antagonist was cloned into the genome of OVV, whose selective replication in cancer cells is associated with cellular EGFR/Ras signaling, thymidine kinase (TK) elevation, and type-I IFN resistance (20, 21). We have chosen an OVV as the delivery vector because the virus has evolved mechanisms for intravenous stability and spread to distant tissues, including resistance to antibody- and complement-mediated neutralization in the blood (22, 23). In addition, the highly destructive nature of a poxvirus infection results in the release of several cellular and viral danger signals, leading to generation of potent inflammatory responses that ultimately overcome tumor-mediated immune suppression to clear the virus (24, 25). Furthermore, complete tumor responses in preclinical models with vaccinia viruses containing deletions of the B18R secreted inhibitor of type-I IFN (26) and *TK* genes were accompanied by immune-mediated protection against tumor rechallenge (27). Oncolytic poxvirus therapy may therefore be considered as a method to achieve vaccination in situ, with the adaptive immune response being able to clear minimal residual disease and provide long-term protection against tumor relapse.

As a template for the virally delivered CXCR4 antagonist, we used the CTCE-9908 dimer corresponding to the N-terminal

Significance

Novel advances in viral oncotherapy require effective direct oncolysis and manipulation of the tumor microenvironment, which has proven to be an important target in cancer treatment. The CXCR4 receptor for the CXCL12 chemokine is one of the key stimuli involved in signaling interactions between tumor cells and their microenvironment, suggesting that inhibition of this pathway by oncolytic viruses expressing the CXCR4 antagonist should increase efficacy over that mediated by oncolysis alone. We are unique in demonstrating that targeting CXCR4 signaling through an oncolytic vaccinia virus yields a significant therapeutic impact against primary and metastatic breast cancer.

Author contributions: M.G., M.S., S.I.A., and D.K. designed research; M.G. and M.P.K. performed research; M.G., M.S., M.P.K., S.I.A., and D.K. analyzed data; and M.G., M.S., S.I.A., and D.K. wrote the paper.

The authors declare no conflict of interest.

This article is a PNAS Direct Submission.

[1]To whom correspondence should be addressed. E-mail: Danuta.Kozbor@roswellpark.org.

This article contains supporting information online at www.pnas.org/lookup/suppl/doi:10.1073/pnas.1220580110/-/DCSupplemental.

region of CXCL12 chemokine (KGVSLSYR-K-RYSLSVGK). This CXCR4 antagonist, the safety of which has been demonstrated in a phase I/II trial in cancer patients (17), is capable of blocking the CXCL12/CXCR4 interaction (28) and delaying the development of metastasis in breast cancer mouse models (29, 30). In the virally delivered construct, the first eight amino acids of CTCE-9908 were expressed in the context of murine (mFc) or human (hFc) fragment of IgG with disulfide bonds in a hinge region for preservation of its dimeric structure (Fig. S1 *A–C*). Using a highly metastatic 4T1 tumor model, which emulates stage IV breast cancer in humans (31), we demonstrated that the virally delivered CXCR4-A-mFc antagonist was predominantly retained in the tumor and inhibited the growth of both primary and metastatic lesions. A systemic delivery of the armed virus after resection of the primary tumor further reduced the development of spontaneous metastasis and resulted in increased tumor-free survival. The OVV-CXCR4-A-mFc antitumor efficacy was associated with destruction of intratumoral microvessels, lower accumulation of CEPs and neutrophils/granulocytic-myeloid derived suppressor cells (G-MDSCs), as well as enhancement of the vaccinia-mediated activation of antitumor antibody responses.

Results

OVV-CXCR4-A-mFc Inhibits Growth of Orthotopic Primary Mammary Tumors. We compared the antitumor efficacies of soluble and virally delivered CXCR4-A-mFc fusion protein against orthotopically growing 4T1 mammary carcinoma in syngeneic female BALB/c mice (n = 6 per group). Intravenous injections of soluble CXCR4-A-mFc fusion protein (25 mg/kg) or 10^8 PFUs of OVV-CXCR4-A-mFc were initiated when the tumor volume was ~150 mm^3 (Fig. 1*A*). This dose of the soluble antagonist was used based on previous studies with the CTCE-9908 dimer that showed a significant reduction in primary tumor growth after daily delivery (5 d/wk) for 5–6 wk (29). In our study, however, the treatment continued for 7 d only to simulate a 1-wk production of the CXCR4-A-mFc protein from OVV-CXCR4-A-mFc–infected tumor cells (32). At 10^8 PFU, OVV-CXCR4-A-mFc was not effective in mobilizing hematopoietic stem and progenitor cells in the peripheral blood (Fig. S1*D*), and did not induce organ injury as assessed by H&E staining of paraffin-embedded tissues (Fig. S2). The soluble CXCR4-A-mFc fusion protein inhibited 4T1 tumor growth during the first 2 wk of the postdelivery period ($P < 0.05$). Then, tumor growth progressed at comparable rates relative to the PBS-treated control mice or to mice receiving an equivalent dose of the mIgG2aFc protein (Fig. 1*B*). In contrast, a single delivery of OVV-CXCR4-A-mFc resulted in dormancy that extended for a period of 3 wk, after which the tumor growth progressed at slower rates compared with control tumors and those treated with a virus expressing the enhanced GFP (OVV-EGFP) (Fig. 1*C*) ($P = 0.002$ and $P = 0.017$, respectively). The latter virus was used as a specificity control and to monitor numbers of $EGFP^+$ cells in tumor tissue during the peak and cessation of viral replication on days 4 and 8, respectively.

To determine whether the enhanced antitumor efficacy of the virally delivered CXCR4-A-mFc protein, compared with its

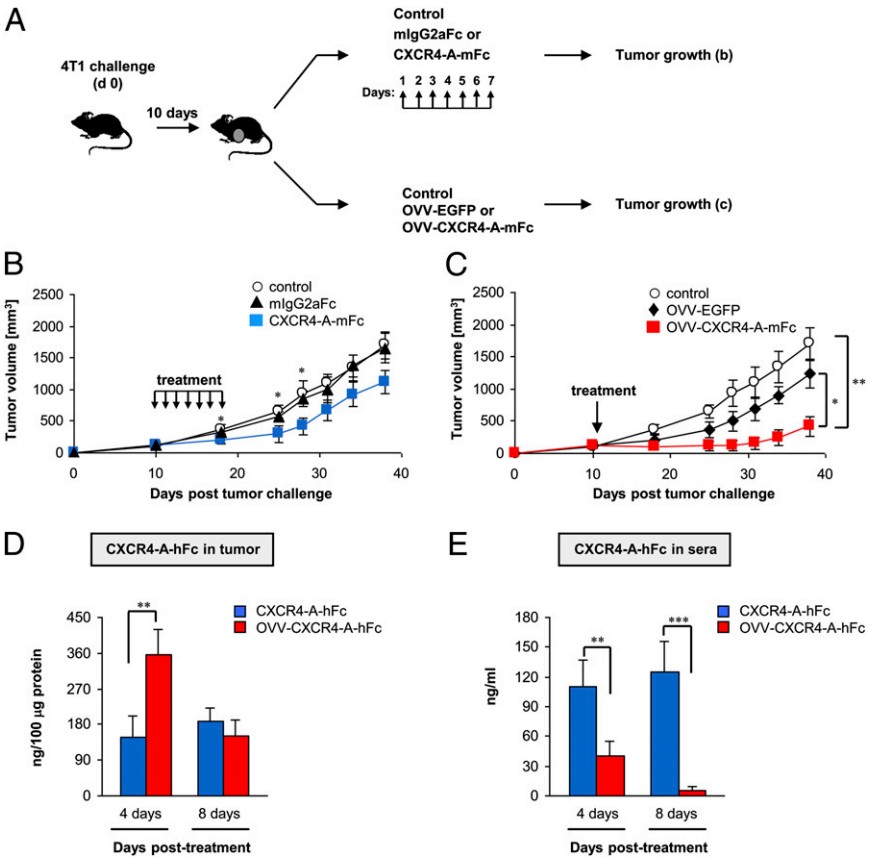

Fig. 1. Inhibition of orthotopic 4T1 tumor growth by soluble and virally delivered CXCR4-A-Fc fusion proteins in BALB/c mice. (*A*) BALB/c mice (n = 6 per group) were inoculated in the thoracic mammary fat pad with 7×10^4 4T1 cells and treated by intravenous injections of the antagonist when the tumor volume was ~150 mm^3. The injections of soluble CXCR4-A-mFc fusion protein or mIgG2aFc protein (25 mg/kg) continued for 7 d, whereas OVV-CXCR4-A-mFc or OVV-EGFP (10^8 PFU) was delivered once. Control mice were injected with PBS (*B* and *C*). Tumor growth was measured one to three times per week with a microcaliper. Concentrations of intratumoral (*D*) and serum (*E*) CXCR4-A-hFc fusion protein were determined by ELISA performed on days 4 and 8 after initiation of treatment. Data are presented as the means ± SD of two independent experiments with three mice per group. $*P < 0.05$, $**P < 0.01$, $***P < 0.001$.

soluble counterpart, was attributed to differences in intratumoral concentrations of the CXCR4 antagonists, we measured the levels of the fusion protein expression in tumor tissues and sera of 4T1 tumor-bearing mice. For this analysis, we used a fusion protein consisting of human instead of murine Fc fragment (CXCR4-A-hFc) to avoid cross-reactivity with murine antibodies in ELISA. The soluble CXCR4-A-hFc antagonist was injected intravenously for 7 d at a concentration of 25 mg/kg, whereas OVV-CXCR4-A-hFc was delivered once at 10^8 PFU. The results depicted in Fig. 1*D* reveal that the intratumoral concentration of virally delivered CXCR4-A-hFc protein at the peak of viral replication (day 4) was >twofold higher compared with that achieved with the soluble counterpart ($P = 0.0016$), and both proteins reached comparable levels on day 8. In the sera, the virally delivered CXCR4-A-hFc protein was detectable only on day 4, which differed from the significantly higher concentrations of the soluble antagonist present on both days (Fig. 1*E*) ($P < 0.01$).

OVV-CXCR4-A-mFc Causes Disruption of Tumor Vasculature. Previous studies with oncolytic virotherapy have demonstrated that in addition to a direct tumor cell killing effect, inflammation induced during the infection triggers tumor vasculature shut-down accompanied by the infiltration of neutrophils/G-MDSCs, intravascular thrombosis, and vascular necrosis (33, 34). To assess the vascular responses to OVV-CXCR4-A-mFc treatment, immunostaining of tumor sections was performed with mAb specific for CD31, a membrane protein of the Ig superfamily that is expressed constitutively on the surface of adult and embryonic endothelial cells (35–37). The analysis was carried out on tumor samples harvested 8 d after the virotherapy treatment. In parallel, the same tissue sections were stained with mAb against the K_i-67 protein, which is expressed in all phases of the cell cycle except G_0 and serves as a valid marker for proliferation (38). The spatial heterogeneity of the response was evaluated by estimating microvessel density (MVD) and K_i-67$^+$ cell numbers in the central (core) and the peripheral (rim) regions of the tumor. As depicted in Fig. 2*A*, *Upper*, control tumors appeared well-vascularized with distinct CD31$^+$ endothelial clusters that were generally more prominent in the periphery than the core (Fig. 2*A*, *Lower*), and were surrounded by actively proliferating K_i-67$^+$ cells (Fig. 2*B, Upper*). Consistent with the previous findings (39), tumor sections from mice treated with OVV-EGFP showed marked vascular damage in the core with significant decreases in MVD and K_i-67$^+$ cells compared with control tumors ($P = 0.024$ and $P = 0.002$, respectively). However, functioning vessels were clearly visible in the viable tumor rim after OVV-EGFP treatment (Fig. 2*A*) along with increased accumulation of K_i-67$^+$ cells ($P = 0.038$) (Fig. 2*B*, *Lower*). In contrast, OVV-CXCR4-A-mFc–treated sections showed extensive areas of necrosis and marked disruption of the vasculature in the tumor periphery compared with OVV-EGFP–treated and control mice ($P < 0.001$). Although no significant MVD differences in the core were observed after OVV-EGFP and OVV-CXCR4-A-mFc treatments, the reductions in viable vessels and numbers of K_i-67$^+$ cells in the rim following OVV-CXCR4-A-mFc

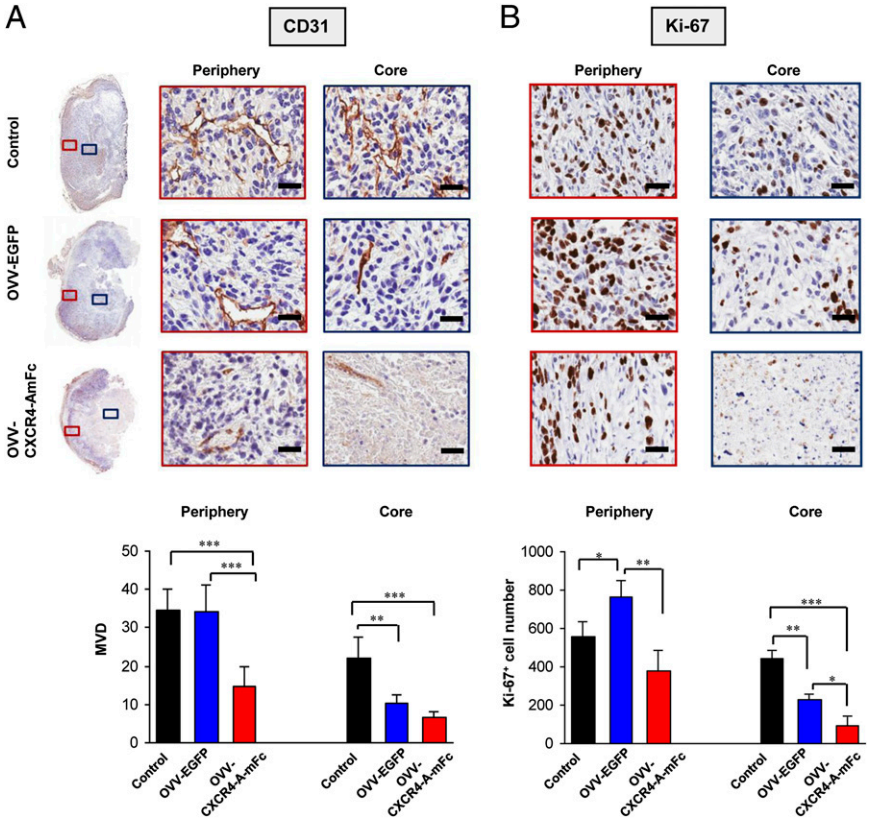

Fig. 2. Assessment of tumor vascular response and cellular proliferation after OVV-CXCR4-A-mFc therapy. (*A*) Photomicrographs of CD31-immunostained whole tumor sections and enlarged images of regions from the tumor periphery and core are shown (*Upper*). Tumors from control mice and those treated with OVV-EGFP or OVV-CXCR4-A-mFc were harvested 8 d after the treatment. Bar graphs show MVD estimates in the tumor periphery and core of sections obtained from control, OVV-EGFP and OVV-CXCR4-A-mFc treated animals (*Lower*). MVD was estimated by calculating the number of CD31$^+$ endothelial clusters on 10–15 fields (20× magnification) from three tumors per group for control and treatment groups. (*B*) Immunohistochemical characterization of proliferative responses by nuclear expression of K_i-67 (*Upper*). The number of K_i-67$^+$ cells was counted in 10 nonoverlapping fields (20× magnification) from control and treatment groups (*Lower*). *$P < 0.05$, **$P < 0.01$, ***$P < 0.001$. (Scale bars, 25 μm.)

delivery were significant compared with OVV-EGFP–treated mice (Fig. 2) ($P < 0.001$ and $P = 0.008$, respectively).

The changes in tumor vasculature after treatments with the armed and OVV-EGFP viruses were also reflected in tumor perfusion visualized by accumulation of fluorescence beads (39). Fluorescence microscopy of tumor sections revealed a relatively uniform distribution of fluorescence beads in the periphery and core of control tumors (Fig. 3*A*). In OVV-EGFP–treated mice, the beads were accumulated predominantly in the periphery (Fig. 3*A*, *Left*) with virtually no perfusion in the core (Fig. 3*A*, *Right*). In contrast, tumor perfusion was markedly reduced both in the rim and core of OVV-CXCR4-A-mFc–treated tumors.

OVV-CXCR4-A-mFc Reduces Intratumoral Expression of CXCL12 and VEGF as Well as Recruitment of CEPs and Neutrophils/G-MDSCs. Given the role of CXCR4/CXCL12 signaling in angiogenesis and vasculogenesis, we next examined if the observed differences in the tumor vascular response to the viruses could be attributed to the inhibitory effects of the CXCR4 antagonist. ELISA analyses of secreted CXCL12 protein in stromal cell-enriched supernatants derived from tumors resected 8 d after oncolytic virotherapy revealed approximately twofold higher levels of CXCL12 protein in the control and OVV-EGFP–treated tumors compared with OVV-CXCR4-A-mFc–treated counterparts (Fig. 3*B*) ($P = 0.003$ and $P = 0.007$, respectively). As depicted in Fig. 3*C*, changes in the CXCL12 expression levels paralleled those of VEGF in tumor lysates. The latter factor, the expression of which is affected by CXCL12 (40), is pivotal in tumor angiogenesis (41, 42). Thus, the increases in CXCL12 and VEGF levels together with higher proliferative indices and MVD suggest a potential angiogenic "rebound" in tumors infected with OVV-EGFP compared with those treated with the armed virus. This possibility is also supported by other findings, which demonstrated that binding of CXCL12 to CXCR4 expressed on endothelial progenitor cells and G-MDSCs triggers migration of CEPs (10, 13) and myeloid cells (14) to the tumor tissues.

The recruitment of CEPs to control and virally treated tumors was examined 8 d after the infection by immunofluorescence staining of single-cell suspensions with mAbs specific for CD45, VEGFR2, and c-kit. Consistent with the decreased tumor vascularization and CXCL12 expression, the intratumoral accumulation of CEPs after treatment with the armed virus was significantly diminished compared with control and OVV-EGFP–treated counterparts (Fig. 3*D*) ($P = 0.047$ and $P = 0.008$, respectively).

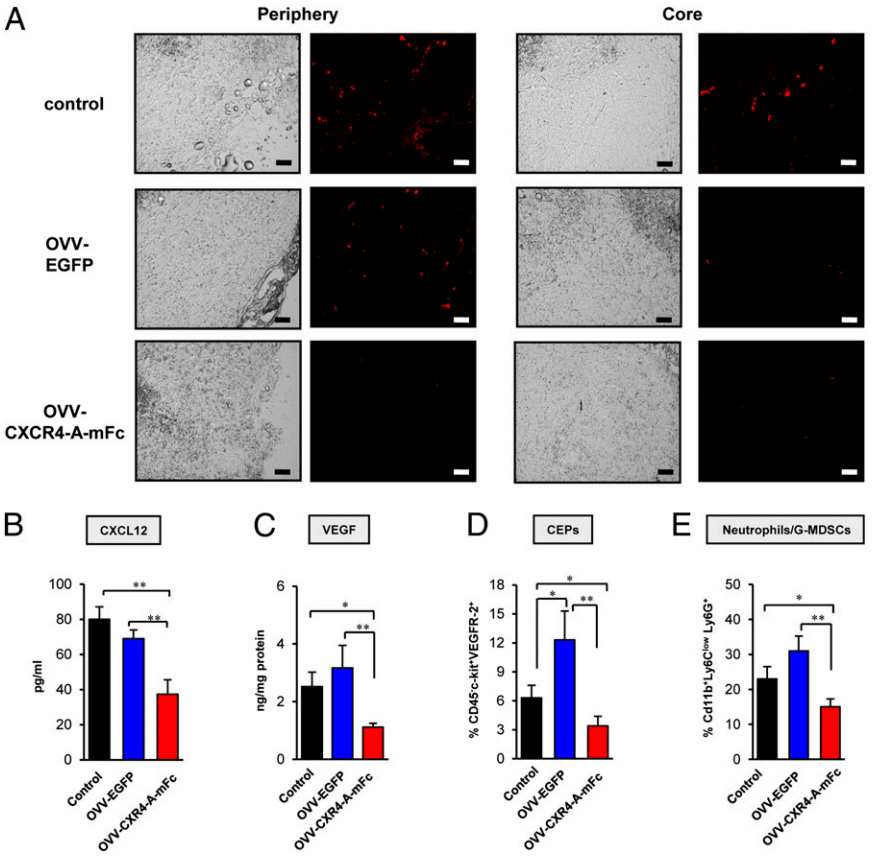

Fig. 3. Tumor perfusion and changes in expression of CXCL12, VEGF, as well as numbers of CEPs and neutrophils/G-MDSCs induced in tumor after oncolytic virotherapy treatment. (*A*) Tumor-bearing mice were injected intravenously with 100 μL of a 50% solution of 100-nm-diameter orange fluorescent microspheres. Five minutes later, animals were killed and tumors were immediately snap-frozen for analyses of tumor perfusion by visualizing fluorescent microspheres in the vasculature of fixed sections using a Zeiss Axiophot HRM Inverted fluorescent microscope and analyzed using Image-Pro-6.2 software. (Scale bars, 100 μm.) (*B*) Intratumoral expression of CXCL12 was determined in tumor stromal cell-enriched supernatants derived from tumors resected on day 8 after the treatment, whereas expression of VEGF (*C*) was determined in tumor lysates as described in *Materials and Methods*. ELISAs were performed on media or lysates and colorimetric values were measured by microplate reader at 450 nm. (*D*) Recruitment of CEPs ($CD45^-$c-$kit^+VEGFR\text{-}2^+$) was determined in control and virally treated tumors with 8 d after treatment. Single-cell suspensions were prepared from 4T1 tumors and stained with anti–CD45-APC-Cy7, anti–VEGFR-2-PerCP-Cy5.5, and anti–c-kit-PE mAbs. (*E*) The percentage of mobilization neutrophils/G-MDSCs in control and treatment groups. Cells were stained with anti-CD11b-APC, anti-Ly6C-FITC, and anti–Ly6G-PE mAbs and analyzed by flow cytometry. Background staining was assessed using isotype control antibodies. Results are presented as the means ± SD of three or four independent experiments. $*P < 0.05$, $**P < 0.01$.

However, the number of CEPs in control tumors was lower than that in OVV-EGFP–infected tumors ($P = 0.036$) despite comparable levels of CXCL12 in both groups of mice (Fig. 3*B*), suggesting that other types of cells with proangiogenic activities could contribute to their recruitment after viral delivery. Notably, some of these cells, such as mobilized granulocytes, could be recruited to the tumor after infection with the unarmed virus promoting angiogenesis by inducing VEGF expression in neoplastic tissue (43).

Because neutrophils/G-MDSCs are one of the first cell types recruited to the sites of infection (44), single-cell suspensions prepared from the virally infected tumors were analyzed for the expression of CD11b, Ly6G, and Ly6C markers by flow cytometry. We focused on cells with high expression of CD11b and Ly6G antigens and low Ly6C levels, as this phenotype represents a population of granulocytes, including neutrophils and G-MDSCs (45). Consistent with the profile of intratumoral CXCL12 and the recent observation that changes mediated by oncolytic virotherapy within tumors may act as a sink for activated neutrophils (33, 46), the highest recruitment of $CD11b^{+}Ly6C^{low}Ly6G^{+}$ cells were detected in tumors after the OVV-EGFP therapy treatment (Fig. 3*E*). The numbers of such myeloid cells were also increased in control tumors, although the differences did not reach statistical significance. In contrast, the accumulation of neutrophils/G-MDSCs in OVV-CXCR4-A-mFc–treated tumors were significantly reduced compared with the control and OVV-EGFP–treated counterparts ($P = 0.042$ and $P = 0.009$, respectively). These findings suggest that the effect of virally delivered CXCR4 antagonist on the CXCL12/CXCR4 signaling axis prevails over the inflammatory capacity of the oncolytic virus in recruitment of neutrophils/G-MDSCs to the tumor microenvironment.

Reduction in Metastatic Disease Following OVV-CXCR4-A-mFc Treatment Is Accompanied by the Induction of Antitumor Antibody Responses. The ability of orthotopically growing 4T1 tumors to disseminate to the lung at early stages of tumor growth (31) allowed us to analyze the efficacy of OVV-CXCR4-A-mFc against lung metastases. Oncolytic virotherapy treatment was initiated once the primary tumors reached ~150 mm^3 and had disseminated into the lungs based on the histological evaluation of formalin-fixed lung sections. Metastatic growth was monitored by bioluminescence for 30 d (Fig. 4*A*, *Upper*). Euthanasia was performed at the time of excessive tumor burden in the control mice, after which lung metastases were histologically assessed in the control and treatment groups. Fig. 4*A*, *Lower* and Fig. 4*B* revealed 18–22 metastatic lesions per section in the lung of control mice, which was significantly higher than the numbers of metastatic colonies after OVV-EGFP therapy (6.6 ± 1.2 SD; $P = 0.001$) and OVV-CXCR4-A-mFc treatment (2.6 ± 0.6 SD; $P = 0.0002$). Furthermore, the numbers of metastatic colonies and the area covered by metastases were significantly reduced in OVV-CXCR4-A-mFc–treated animals compared with those treated with the virus only ($P = 0.04$ and $P = 0.01$, respectively).

The reduced metastatic burden in the lungs after OVV-EGFP treatment could be accounted by a direct cytotoxic effect of the virus as well as the induction of antitumor immunity because of the ability of vaccinia virus to break $CD4^{+}$ $CD25^{+}$ regulatory T-cell–mediated tolerance through Toll-like receptor (TLR)-dependent and -independent pathways (24, 25), and augment the efficacy of a cancer vaccine composed of dendritic cells pulsed with an IL-2 gene-encoded vaccinia virus tumor oncolysate (47). To investigate whether targeting of the tumor by OVV-EGFP was associated with the generation of antitumor immunity, sera were collected from the same mice that had been examined for the lung metastases at several time-points, including before tumor challenge, at the time of orthotopic 4T1 inoculation, at the time of therapy, and every 10 d until killing (Fig. 4 *B* and *C*). The sera specimens were analyzed for the presence of antibodies to ALCAM/CD166 tumor associated antigen (TAA) expressed by 4T1 cells in ELISA using wells coated with the 47-LDA peptide mimic of GD2 ganglioside (48) that cross-reacts with ALCAM/CD166 (49). The 47-LDA mimotope was capable of inducing antitumor immunity in tumor-bearing mice when delivered either as a dendritic cell vaccine or by OVV-47-LDA-Fcγ2a vector (50).

At the serum dilution of 1:100, control mice exhibited a background level of reactivity throughout the entire study, reflecting the inability of the tumor-bearing mice to mount antitumor responses (Fig. 4*C*). In contrast, antitumor antibodies were detected in both OVV-EGFP- and OVV-CXCR4-A-mFc–treated mice within a week after the respective treatment. In OVV-EGFP–treated mice, the antibodies were present in two of three mice and rapidly declined within ~25 d. The antibodies were generally higher and more sustained in OVV-CXCR4-A-mFc–treated mice. This result was clearly evident at the end of the study in mice with a lower metastatic load, suggesting that the initial vaccinia virus-mediated antitumor response was augmented by CXCR4-A-mFc–mediated changes in the tumor microenvironment.

Perioperative Treatment with OVV-CXCR4-A-mFc Improves Overall Survival and Confers Resistance to Tumor Rechallenge. The efficacy of OVV-CXCR4-A-mFc therapy in sites of established micrometastases in the lungs was examined when the oncolytic therapy treatments were administered either before or after excision of the primary tumor. In the preoperative setting, 4T1 tumor-bearing mice received oncolytic virotherapy 10 d after tumor challenge, which roughly corresponded to a tumor volume of 150 mm^3, followed by resection of the primary tumor 8 d later (Fig. 5*A*, *Left*). This treatment facilitated replication of the virus in both primary (5.1 ± 3.9 $\log_{10}$ PFU/mg total protein) and metastatic tumors (1.8 ± 1.1 $\log_{10}$ PFU/mg total protein), as determined 4 d after viral challenge by a standard plaque assay. As shown in Fig. 5*A*, *Right*, this combination therapy prolonged survival of both OVV-EGFP and OVV-CXCR4-A-mFc–treated mice compared with control mice ($P = 0.049$ and $P = 0.0011$, respectively). Importantly, resection of the primary tumor improved the antitumor efficacy of the armed virus as 20% of animals remained disease-free for a period longer than 110 d.

We next examined the efficacy of the oncolytic virotherapy in a postoperative setting, wherein the primary tumors were resected 18 d after tumor challenge, before the viral delivery (Fig. 5*B*, *Left*). In these mice, the viral titer in the lung metastases (2.5 ± 1.3 $\log_{10}$ PFU/mg total protein) was significantly higher compared with that in the preoperative setting ($P = 0.005$), suggesting that excision of the primary tumor before oncolytic virotherapy would enable higher viral replication in the metastatic lesions and contribute to the improved treatment efficacy. As shown in Fig. 5*B*, *Right*, the survival of OVV-CXCR4-A-mFc–treated mice was significantly higher than control and OVV-EGFP–treated animals ($P = 0.0007$ and $P = 0.023$, respectively), and 42% of mice remained tumor-free. Notably, all tumor-free mice exhibited 47-LDA antibody responses (mean titer $1{:}720 \pm 180$) and significant resistance to 4T1 tumor rechallenge based on a delay or lack of tumor growth compared with their naive counterparts (Fig. 5*C*) ($P = 0.0007$).

Discussion

Although engineered OVVs have demonstrated promising results in the treatment of cancer in preclinical models and early clinical trials (21, 51), systemic efficacy against metastatic disease needs to be improved to have a major impact on cancer patient survival. Furthermore, there is a limited understanding of the viral interaction with different elements of tumor stroma, which could be used to improve therapeutic outcome of the given treatment. Because the CXCR4 receptor for the CXCL12 chemokine is one of the key stimuli involved in signaling interactions between tumor cells and their microenvironment, we hypothesized that targeting

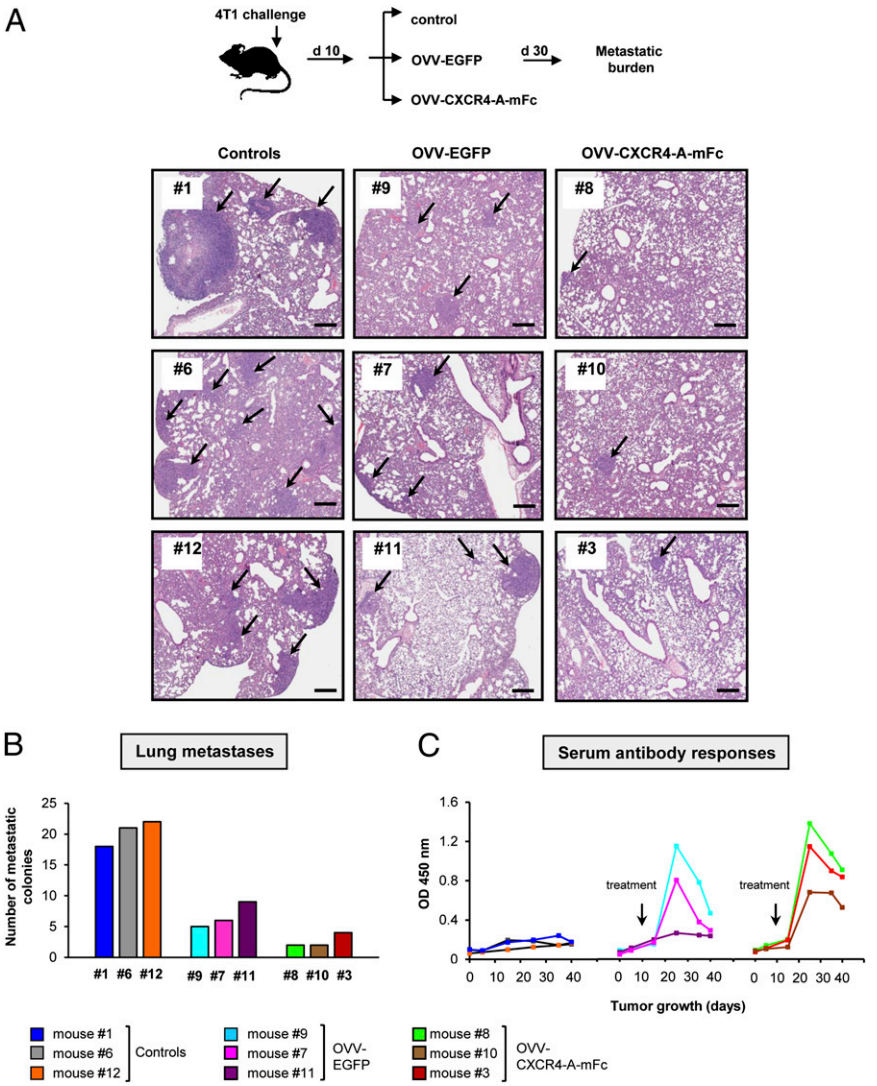

Fig. 4. Evaluation of lung metastases and antibody responses in mice after onvolytic virotherapy. (*A*) The oncolytic virotherapy was initiated once the primary tumor reached ~150 mm^3 (n = 3 mice per group). Metastatic growth in control and treatment groups were monitored by bioluminescence for 30 d until killing was performed at the time of excessive tumor burden in control mice (*Upper*), after which lung metastases were assessed by histology on formalin-fixed and H&E-stained sections (*Lower*). (Scale bars, 300 μm.) (*B*) Numbers of metastatic colonies per section were presented in individual mice. (*C*) Sera collected before tumor challenge, at the time of orthotopic 4T1 challenge, at the time of treatment, and every 10 d until killing were analyzed for the presence of antitumor antibody responses by ELISA using wells coated with 47-LDA mimotope of ALCAM/CD166. All samples were analyzed in triplicates with serum dilution of 1:100.

the CXCR4 pathway with oncolytic viruses would result in tumor growth inhibition and increase the efficacy of therapeutic vaccinations. We show that a CXCR4 antagonist delivered intravenously by an OVV attains higher intratumoral concentrations than its soluble counterpart and results in a systematically effective virus with increased efficacy over that mediated by the oncolysis alone. To our knowledge, we are unique in showing that targeting the CXCL12/CXCR4 signaling axis through an oncolytic virus yields significant antitumor activity against primary and metastatic mammary cancer. In particular, treatment with OVV-CXCR4-A-mFc after resection of the primary tumor led to a marked improvement in overall disease-free survival.

We established that the higher antitumor efficacy of OVV-CXCR4-A-mFc compared with that mediated by the unarmed virus expressing EGFP was associated with destruction of tumor vasculature in the periphery, as well as lower intratumoral accumulation of bone marrow-derived CEPs and neutrophils/G-MDSCs. Although CEPs are known to home to the vasculature of treated tumors and promote tumor neovascularization (52), G-MDSCs were reported to change the premetastatic lung into an inflammatory and proliferative environment, diminish immune protection, and promote metastasis through aberrant vasculature formation (53). Thus, inhibition of angiogenesis and vasculogenesis in tumors treated with the armed virus together with the direct cytopathic effect of the virus on the malignant population could contribute to a lower metastatic burden in the lungs. It is also possible that the CXCR4-A-mFc antagonist could directly interfere with the CXCL12/CXCR4 axis in 4T1 cells, as knockdown of CXCR4 in tumor cells or treatment with CXCR4 antagonists limited orthotopic primary tumor growth as well as tumor metastasis (54, 55). The Fc fragment of CXCR4-A-mFc could also induce complement-dependent cytotoxicity of the fusion protein-coated 4T1 cells (56), trigger phagocytosis by neutrophils and macrophages (57), and activate NK cells to lyse tumor cells (58). Our studies in tumor-free mice after the OVV-CXCR4-A-mFc treatment revealed the presence of complement-mediated lysis of

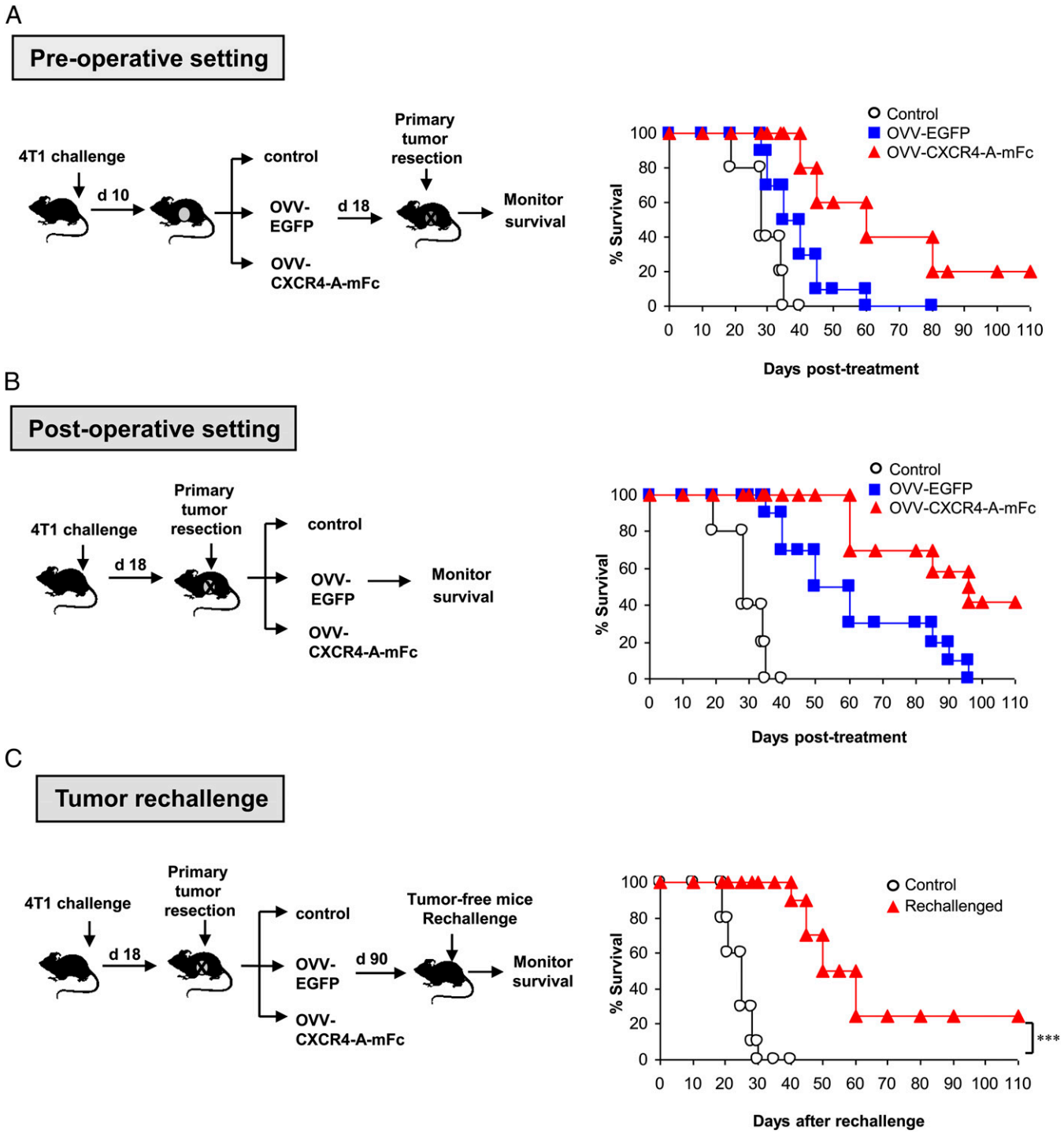

Fig. 5. Perioperative treatment with OVV-CXCR4-A-Fc facilitates overall survival and resistance to tumor rechallenge. (*A*) In the preoperative setting, 4T1-bearing mice (n = 8–12 per group) received oncolytic viriotherapy 10 d after tumor challenge, which roughly corresponded to a tumor volume of 150 mm^3, followed by resection of the primary tumor 8 d later. Control mice were treated with PBS before excision of the primary tumor. (*B*) In the postoperative setting, the oncolytic virotherapy treatment was initiated after resection of the primary tumor on day 18. (*C*) Tumor-specific immune memory responses protected mice from 4T1 rechallenge. Tumor-free mice after treatment with OVV-CXCR4-A-mFc were rechallenged orthotopically with 4T1 cells. Naive mice challenged with 4T1 tumor served as controls. Animals were examined daily until the tumor became palpable, after which tumor growth was measured as in Fig. 1. Survival was defined as the point at which mice were killed because of extensive tumor burden (i.e., experimental/humane endpoints). Kaplan–Meier survival plots were prepared, and significance was determined using the log-rank method. ***$P < 0.001$.

CXCR4-A-mFc–coated 4T1 cells (Fig. S3*A*). The fusion protein-coated 4T1 cells were also susceptible to antibody-dependent cell-mediated cytotoxicity responses against CXCR4-A-mFc–coated 4T1 cells by NK cell-enriched splenocytes isolated from tumor-free mice (Fig. S3*B*). Additional experiments with a CXCR4-negative variant of 4T1 tumor cells will aid to dissect the effect of OVV-CXCR4-A-mFc–targeted CXCR4 expression by stromal cells on primary and metastatic tumor growth.

The induction of antitumor antibody responses during the oncolytic virotherapy treatment, together with the resistance of OVV-CXCR4-A-mFc–treated mice to tumor rechallenge, holds important implications for immunotherapy, as immune suppression within the tumor stroma may be a major determinant of the poor outcome of therapeutic vaccinations. Because vaccinia virus-based vaccines have been shown to elicit innate immunity through the TLR2/MyD88-dependent pathway and TLR-independent production of IFN-β (25), this ability of the virus to provide persistent TLR signals for immunotherapy in a setting of established tolerance, together with the CXCR4 antagonist-mediated changes in the tumor microenvironment, could induce a more sustained level of antitumor antibody responses. Additional studies are in progress to improve the longevity of the antibody responses directed to the 47-LDA mimotope of ALCAM/CD166 antigen in OVV-CXCR4-A-Fc–treated mice for long-lasting protection against metastasis. The presence of strong and sustained antibodies to ALCAM/CD166 might be relevant in view that ALCAM/CD166 regulates matrix metalloproteinase activity (MMP) and acts as a cell sensor for cell density, controlling the transition between local cell proliferation and tissue invasion (59). Expression of ALCAM/CD166 and MMP-2 activation correlates with metastatic potential in human melanoma cells (60), and high ALCAM/CD166 expression in primary breast carcinomas has been suggested to be a suitable marker for prediction of the response to adjuvant chemotherapy and a potential target for therapy (61).

In conclusion, our studies have shown increased antitumor efficacy of the targeted delivery of the CXCR4-A-mFc antagonist by OVV against primary tumors and spontaneous metastases compared with the conventional drug delivery approach. This innovative immune-based technology opens up the possibility of engineered oncolytic viruses, which selectively infect tumor cells and express high concentrations of therapeutic molecules in metastatic tumors to potentiate the eradication of cancer.

Materials and Methods

Animals and Cell Lines. Female BALB/c mice, 6–8 wk of age, were obtained from the National Cancer Institute-Frederick Animal Production Program. The experimental procedures were performed in compliance with protocols approved by the Institutional Animal Care and Use Committee of the Roswell Park Cancer Institute. The murine 4T1 breast carcinoma (62), human HuTKP^{-}P 143 fibroblasts, human cervical carcinoma HeLa cells (63), and monkey kidney fibroblasts CV1 (64) were obtained from the American Type Culture Collection.

Vaccinia Viruses. All vaccinia viruses used in this study are of the Western Reserve strain with disrupted *TK* and vaccinia growth factor (*VGF*) genes for enhanced cancer cell specificity. OVV were created by homologous recombination of EGFP and the CXCR4-A-Fc fusion protein into the *TK* gene of VSC20 vaccinia using the shuttle plasmids pSEL-EGFP and pCB023-CXCR4-A-Fc, respectively. The parental VSC20 vaccinia virus with *lacZ* gene cloned in place of the *VGF* gene (65) was obtained from Bernard Moss (National Institutes of Health, Bethesda, MD). The pCB023 and pSEL-EGFP vaccinia shuttle plasmids (66) were obtained from David Bartlett (University of Pittsburgh Cancer Institute, Pittsburgh, PA). To generate the CXCR4-A-Fc fusion proteins, Fc fragments of mouse IgG2a and human IgG1 were cloned in-frame with the annealed oligonucleotides AAGGGAGTCAGCCTGAGCTACAGA corresponding to the CTCE-9908 peptide antagonist (30) into the EcoRI and BglII restriction enzyme cleavage sites of the respective pFUSE-mIgG2A-Fc2 and pINFUSE-hIgG1-Fc2 vectors (InvivoGen) (Fig. S1*A*). The transgenes were subcloned into the SalI and XbaI restriction enzyme sites of the pCB023 plasmid under control of the vaccinia synthetic early/late promoter Pse/I (67). The inserted fusion protein genes were flanked by portions of *TK* gene that allowed for the homologous recombination of CXCR4-A-Fc into *TK* locus of VSC20. Confluent wells of CV1 cells were infected for 2 h at 37 °C with 1.4×10^5 PFU of VSC20 in 1.0 mL of MEM-2.5% (vol/vol) FCS. Supernatants were removed, and a liposomal transfection (Invitrogen) of pCB023-CXCR4-A-Fc was performed according to the manufacturer's protocol. Multiple plaques of the recombinant viruses were isolated on a monolayer of HuTKP^{-}P 143 fibroblasts by BrdU selection. The construction of pSEL-EGFP vaccinia shuttle plasmid encoding *EGFP* gene under control of Pse/I promoter as well as the generation of OVV-EGFP by homologous recombination of EGFP into *TK* gene of VSC20 vaccinia have been previously described (50, 66). The OVV-CXCR4-A-mFc, OVV-CXCR4-A-hFc and OVV-EGFP viruses were amplified on HeLa cells, purified over the sucrose gradient, titered, and used for in vitro and in vivo studies. The fusion proteins were collected in supernatants of infected HuTKP^{-}P 143 cells and purified on protein G column before 10% SDS/PAGE. Western blotting of the purified CXCR4-A-m/hFc fusion proteins using the Fc fragment-specific peroxidase-conjugated antibodies followed by ECL plus Western blotting detection system (Amersham Biosciences/GE Healthcare) was performed under nonreducing and reducing conditions (Fig. S1 *B* and *C*). The expression of EGFP in OVV-EGFP–infected 4T1 cells was confirmed by immunofluorescence microscopy.

To determine the titer of vaccinia viruses in primary and metastatic tumors, tissues were resected on day 4 after infection, homogenized, and titrated by a standard plaque assay. Plaques were counted by visual inspection.

In Vivo Studies. Female 6-wk-old BALB/c mice (n = 6 per group) were inoculated in the thoracic mammary fat pads with 7×10^4 4T1 cells. Tumor-bearing mice with tumor volumes of ~150 mm^3 were injected intravenously with 10^8 PFU of OVV-EGFP or OVV-CXCR4-A-mFc. A separate group of 4T1-mice were injected with soluble CXCR4-A-mFc fusion protein or mIgG2aFc fragment (25 mg/kg) for 7 d. To analyze the level of CXCR4-A-hFc protein in tumor lysates and sera, tumors and blood samples were harvested 4 and 8 d after each treatment to measure concentrations of the antagonist by ELISA. Tumor growth was monitored by measuring subcutaneous tumors one to three times a week with a microcaliper. The tumor volume, V, was calculated with the formula $V = (lw2/2)$, where l is the longest axis of the tumor and w is the axis perpendicular to l. Tumors were monitored until they reached ~1,700 mm^3, at which time the mice were killed.

The efficacy of OVV-CXCR4-A-mFc therapy against established lung micrometastases was evaluated when oncolytic virotherapy treatment was administered either before or after resection of the primary tumor. For these experiments, 4T1 cells were transfected with pcDNA3.1 vector expressing *Renilla* luciferase (RL) obtained from B. Johnson (Department of Pediatrics, Medical College of Wisconsin, Milwaukee, WI) and stable clones were selected in 100 μg/mL of hygromycin B (Invitrogen). The 4T1-RL transfectants were grown in the presence of hygromycin B until tumor challenge. Metastatic growth was monitored by bioluminescence imaging using Imaging System (IVIS Xenogen, Caliper Life Sciences) after injection of 100 μL of coelenterazine (0.7 μg/kg body weight; Prolume) via tail-vein. Survival was defined as the point at which mice were killed because of extensive tumor burden.

Flow Cytometry. The phenotypic analysis of stromal cells were performed on single cell suspensions prepared from tumors harvested on days 4 and 8 after oncolytic virotherapy with rat mAbs: anti-CD11b-APC, anti-Ly6C-FITC, anti-Ly6G-PE, anti-CD45-APC-Cy7, anti-VEGFR-2-PerCP-Cy5.5 (BD Pharmingen), anti–c-kit-PE (Abcam). Background staining was assessed using isotype control antibodies (BD Pharmingen). Before specific antibody staining, cells were incubated with Fc blocker (anti-CD16/CD32 mAb) for 10 min. All evaluations were performed on FACScalibur flow cytometer (Becton Dickinson). After gating on forward and side-scatter parameters, at least 10,000 gated events were routinely acquired and analyzed using CellQuest software (Becton Dickinson Immunocytometry System).

ELISA. The levels of CXCR4-A-hFc fusion protein in tumor lysates and sera were analyzed by ELISA. In brief, tumors harvested 4 and 8 d after treatment initiation were homogenized, sonicated for 60 s in 1 mL of complete lysis buffer (0.5 NaCl, 10 mM Tris•HCl, 0.5% Nonidet P-40, 1 mM PMSF), and maintained under constant agitation for 1 h at 4 °C. After spinning at 10,000 × g at 4 °C, the serially-diluted lysates were analyzed for the level of CXCR4-A-hFc fusion protein on wells coated with goat anti-human IgG (3 μg/mL; MP Biomedicals). After incubation at room temperature for 2 h, the plates were washed, incubated with a 1:2,000 dilution of peroxidase-conjugated goat anti-human Fc fragment-specific IgG (Sigma), developed with 3,3′,5,5′-tetramethyl-benzidine (0.1 mg/mL; Sigma), followed by 0.2 M sulfuric acid, and analyzed at 450 nm with an ELISA plate reader (Bio-Tek Instruments). For the analysis of the VEGF expression, tumors were harvested 8 d after treatment and total protein concentration in tumor lysates was determined by Bradford assay (68). The tumor lysates were adjusted to 1 mg of total protein content and analyzed by mouse VEGF Alpha Elisa kit (Antigenix America) according to the manufacturer's instructions.

To analyze levels of CXCL12 in stromal cell-enriched supernatants, tumor tissues were digested with collagenase type I (1 mg/mL; Boehringer Mannheim) and hyaluronidase (125 units/mL; Sigma), incubated without shaking for 5 min

at room temperature, followed by the separation of stomal cell-enriched supernatant to a new tube and centrifugation at 250 × *g* for 5 min, as previously described (10). The cells were plated on tissue culture plates and cultured for 48 h. Media containing equal amount of protein (100 μg) were analyzed in ELISA by using CXCL12/SDF-1α Elisa Quantikine kit (R&D Systems).

To measure the levels of antibodies specific for the 47-LDA mimotope of ALCAM/CD166 TAA in sera of the tumor-bearing mice, wells were coated with 47-LDA peptide (AAPPTec; 3 μg/mL) and ELISA was performed with serum dilution of 1:100, as previously described (48). The peptide 47-LDA, recognized by polyclonal rabbit anti-ALCAM/CD166 antibody (Santa Cruz), was originally isolated from a phage display peptide library with 14G2a mAb to GD2 ganglioside (48) that cross-reacts with ALCAM/CD166 (49).

Immunohistochemistry. Tumors harvested with adjacent skin were placed immediately in Tris-buffered zinc fixative (0.1 M Tris•HCl buffer (pH 7.4) containing 3.2 mM calcium acetate, 22.8 mM zinc acetate, and 36.7 zinc chloride) for 6–18 h, transferred to 70% ethanol, dehydrated, and embedded in paraffin. Sections (5-μm-thick) were stained by a routine immunohistochemical method using a rat mAb specific for CD31 (MEC 13.3; BD Pharmingen) at 1:50 dilution in PBS for 60 min at 37 °C, followed by biotinylated rabbit antirat IgG (BD Pharmingen) at 1:100 dilution for 30 min, streptavidin-peroxidase (Zymed) for 30 min, and diaminobenzidine for 5 min. Slides were counterstained with Harris hematoxilin. MVD was estimated by calculating the number of $CD31^+$ endothelial clusters on 10–15 fields (20× magnification) from three tumors per group for control and treatment groups. The same slides were stained with rabbit anti-mouse K_i-67 mAb (SP6; Thermo Scientific) at 1:200 dilutions in PBS for 60 min at 37 °C after antigen retrieval. Biotinylated goat anti-rabbit IgG (Vector) secondary antibody was applied, followed by the Elite ABC Kit (Vectastain), and the DAB chromogen. Slides were counterstained with Hematoxylin, and number of K_i-67^+ cells was counted in 10 nonoverlapping fields (20× magnification).

Analysis of Tumor Perfusion. Tumor-bearing mice were injected intravenously with 100 μL of a 50% solution of 100-nm-diameter orange fluorescent microspheres (Molecular Probes). Five minutes later, animals were killed and the tumors were immediately snap-frozen as described previously (33). Tumor perfusion was analyzed by visualizing fluorescent microspheres in the vasculature of fixed sections using a Zeiss Axiophot HRM Inverted fluorescent microscope (Zeiss) and analyzed with Image-Pro-6.2 software (Media Cybernetics).

Histologic Assessment of Lung Metastases. Animals were humanely euthanized and lungs were removed and placed in 10% formalin for histology. Slides with H&E-stained sections of lungs from control and treated animals were scanned and digitized using the Scanscope XT system and images of lung sections were captured using the ImageScope software (Aperio Technologies). Metastatic deposits were manually traced using the medical imaging software, Analyze (AnalyzeDirect). Total number of nodules and extent of metastatic burden (number of voxels) were calculated from three animals per group in a blinded manner.

Statistical Analyses. The statistical significance of the difference between groups was performed using the two-tailed Student *t* test assuming equal variance. Mixed-model ANOVA was used to compare tumor growth in different groups of mice. The *P* values for the pairwise group comparisons for the average tumor growth were computed using a repeated-measure ANOVA. Differences in MVD between groups were analyzed for statistical significance by one-way ANOVA. $P < 0.05$ was considered statistically significant. Kaplan–Meier survival plots were prepared and median survival times were determined for tumor-challenged groups of mice. Statistical differences in the survival across groups were assessed using the logrank Mantel-Cox method. Data were presented as arithmetic mean ± SD and analyzed using JMP (SAS Institute) on a Windows-based platform.

ACKNOWLEDGMENTS. We thank Drs. Michael Nemeth, Bernard Moss, and David Bartlett for reagents, and Dr. Hans Minderman for assistance with tumor perfusion study and Pathology Core immunohistochemistry. This work was funded in part by the National Institutes of Health Grants CA164475, CA140886, and EB008071 (to D.K.), and CA140622 (to S.I.A.); the Roswell Park Alliance Foundation (D.K. and M.S.); and Comprehensive Cancer Center Support Grant CA16056.

1. Müller A, et al. (2001) Involvement of chemokine receptors in breast cancer metastasis. *Nature* 410(6824):50–56.
2. Kato M, Kitayama J, Kazama S, Nagawa H (2003) Expression pattern of CXC chemokine receptor-4 is correlated with lymph node metastasis in human invasive ductal carcinoma. *Breast Cancer Res* 5(5):R144–R150.
3. Kang H, Watkins G, Douglas-Jones A, Mansel RE, Jiang WG (2005) The elevated level of CXCR4 is correlated with nodal metastasis of human breast cancer. *Breast* 14(5):360–367.
4. Salvucci O, et al. (2006) The role of CXCR4 receptor expression in breast cancer: A large tissue microarray study. *Breast Cancer Res Treat* 97(3):275–283.
5. Woo SU, Bae JW, Kim CH, Lee JB, Koo BW (2008) A significant correlation between nuclear CXCR4 expression and axillary lymph node metastasis in hormonal receptor negative breast cancer. *Ann Surg Oncol* 15(1):281–285.
6. Chu QD, et al. (2010) High chemokine receptor CXCR4 level in triple negative breast cancer specimens predicts poor clinical outcome. *J Surg Res* 159(2):689–695.
7. Bleul CC, Fuhlbrigge RC, Casasnovas JM, Aiuti A, Springer TA (1996) A highly efficacious lymphocyte chemoattractant, stromal cell-derived factor 1 (SDF-1). *J Exp Med* 184(3):1101–1109.
8. Burger JA, Kipps TJ (2006) CXCR4: A key receptor in the crosstalk between tumor cells and their microenvironment. *Blood* 107(5):1761–1767.
9. Liao D, Luo Y, Markowitz D, Xiang R, Reisfeld RA (2009) Cancer associated fibroblasts promote tumor growth and metastasis by modulating the tumor immune microenvironment in a 4T1 murine breast cancer model. *PLoS ONE* 4(11):e7965.
10. Orimo A, et al. (2005) Stromal fibroblasts present in invasive human breast carcinomas promote tumor growth and angiogenesis through elevated SDF-1/CXCL12 secretion. *Cell* 121(3):335–348.
11. Teicher BA, Fricker SP (2010) CXCL12 (SDF-1)/CXCR4 pathway in cancer. *Clin Cancer Res* 16(11):2927–2931.
12. Scotton CJ, et al. (2002) Multiple actions of the chemokine CXCL12 on epithelial tumor cells in human ovarian cancer. *Cancer Res* 62(20):5930–5938.
13. Orimo A, Weinberg RA (2006) Stromal fibroblasts in cancer: A novel tumor-promoting cell type. *Cell Cycle* 5(15):1597–1601.
14. Liu BY, et al. (2010) Stromal cell-derived factor-1/CXCL12 contributes to MMTV-Wnt1 tumor growth involving Gr1+CD11b+ cells. *PLoS ONE* 5(1):e8611.
15. Wald O, et al. (2006) CD4+CXCR4highCD69+ T cells accumulate in lung adenocarcinoma. *J Immunol* 177(10):6983–6990.
16. Devine SM, et al. (2004) Rapid mobilization of CD34+ cells following administration of the CXCR4 antagonist AMD3100 to patients with multiple myeloma and non-Hodgkin's lymphoma. *J Clin Oncol* 22(6):1095–1102.
17. Wong D, Korz W (2008) Translating an antagonist of chemokine receptor CXCR4: From bench to bedside. *Clin Cancer Res* 14(24):7975–7980.
18. Gupta SK, Pillarisetti K (1999) Cutting edge: CXCR4-Lo: Molecular cloning and functional expression of a novel human CXCR4 splice variant. *J Immunol* 163(5):2368–2372.
19. Broxmeyer HE, et al. (2005) Rapid mobilization of murine and human hematopoietic stem and progenitor cells with AMD3100, a CXCR4 antagonist. *J Exp Med* 201(8):1307–1318.
20. Breitbach CJ, et al. (2011) Intravenous delivery of a multi-mechanistic cancer-targeted oncolytic poxvirus in humans. *Nature* 477(7362):99–102.
21. Kirn DH, Thorne SH (2009) Targeted and armed oncolytic poxviruses: A novel multi-mechanistic therapeutic class for cancer. *Nat Rev Cancer* 9(1):64–71.
22. Vanderplasschen A, Mathew E, Hollinshead M, Sim RB, Smith GL (1998) Extracellular enveloped vaccinia virus is resistant to complement because of incorporation of host complement control proteins into its envelope. *Proc Natl Acad Sci USA* 95(13):7544–7549.
23. Vanderplasschen A, Hollinshead M, Smith GL (1997) Antibodies against vaccinia virus do not neutralize extracellular enveloped virus but prevent virus release from infected cells and comet formation. *J Gen Virol* 78(Pt 8):2041–2048.
24. Yang Y, Huang CT, Huang X, Pardoll DM (2004) Persistent Toll-like receptor signals are required for reversal of regulatory T cell-mediated CD8 tolerance. *Nat Immunol* 5(5):508–515.
25. Zhu J, Martinez J, Huang X, Yang Y (2007) Innate immunity against vaccinia virus is mediated by TLR2 and requires TLR-independent production of IFN-beta. *Blood* 109(2):619–625.
26. Alcamí A, Symons JA, Smith GL (2000) The vaccinia virus soluble alpha/beta interferon (IFN) receptor binds to the cell surface and protects cells from the antiviral effects of IFN. *J Virol* 74(23):11230–11239.
27. Kirn DH, Wang Y, Le Boeuf F, Bell J, Thorne SH (2007) Targeting of interferon-beta to produce a specific, multi-mechanistic oncolytic vaccinia virus. *PLoS Med* 4(12):e353.
28. Hassan S, et al. (2011) CXCR4 peptide antagonist inhibits primary breast tumor growth, metastasis and enhances the efficacy of anti-VEGF treatment or docetaxel in a transgenic mouse model. *Int J Cancer* 129(1):225–232.
29. Huang EH, et al. (2009) A CXCR4 antagonist CTCE-9908 inhibits primary tumor growth and metastasis of breast cancer. *J Surg Res* 155(2):231–236.
30. Richert MM, et al. (2009) Inhibition of CXCR4 by CTCE-9908 inhibits breast cancer metastasis to lung and bone. *Oncol Rep* 21(3):761–767.
31. Bao L, et al. (2011) Increased expression of P-glycoprotein is associated with doxorubicin chemoresistance in the metastatic 4T1 breast cancer model. *Am J Pathol* 178(2):838–852.
32. Puhlmann M, et al. (2000) Vaccinia as a vector for tumor-directed gene therapy: Biodistribution of a thymidine kinase-deleted mutant. *Cancer Gene Ther* 7(1):66–73.
33. Breitbach CJ, et al. (2007) Targeted inflammation during oncolytic virus therapy severely compromises tumor blood flow. *Mol Ther* 15(9):1686–1693.

34. Liu TC, Galanis E, Kirn D (2007) Clinical trial results with oncolytic virotherapy: A century of promise, a decade of progress. *Nat Clin Pract Oncol* 4(2):101–117.
35. Newman PJ, et al. (1990) PECAM-1 (CD31) cloning and relation to adhesion molecules of the immunoglobulin gene superfamily. *Science* 247(4947):1219–1222.
36. Albelda SM (1991) Endothelial and epithelial cell adhesion molecules. *Am J Respir Cell Mol Biol* 4(3):195–203.
37. Vanzulli S, et al. (1997) Detection of endothelial cells by MEC 13.3 monoclonal antibody in mice mammary tumors. *Biocell* 21(1):39–46.
38. Scholzen T, Gerdes J (2000) The Ki-67 protein: From the known and the unknown. *J Cell Physiol* 182(3):311–322.
39. Gil M, et al. (2011) Photodynamic therapy augments the efficacy of oncolytic vaccinia virus against primary and metastatic tumours in mice. *Br J Cancer* 105(10):1512–1521.
40. Liang Z, et al. (2007) CXCR4/CXCL12 axis promotes VEGF-mediated tumor angiogenesis through Akt signaling pathway. *Biochem Biophys Res Commun* 359(3):716–722.
41. Ferrara N (2004) Vascular endothelial growth factor as a target for anticancer therapy. *Oncologist* 9(Suppl 1):2–10.
42. Ferrara N (2004) Vascular endothelial growth factor: Basic science and clinical progress. *Endocr Rev* 25(4):581–611.
43. Nozawa H, Chiu C, Hanahan D (2006) Infiltrating neutrophils mediate the initial angiogenic switch in a mouse model of multistage carcinogenesis. *Proc Natl Acad Sci USA* 103(33):12493–12498.
44. Nathan C (2006) Neutrophils and immunity: Challenges and opportunities. *Nat Rev Immunol* 6(3):173–182.
45. Youn JI, Collazo M, Shalova IN, Biswas SK, Gabrilovich DI (2012) Characterization of the nature of granulocytic myeloid-derived suppressor cells in tumor-bearing mice. *J Leukoc Biol* 91(1):167–181.
46. Breitbach CJ, et al. (2011) Targeting tumor vasculature with an oncolytic virus. *Mol Ther* 19(5):886–894.
47. Jack AM, Aydin N, Montenegro G, Alam K, Wallack M (2007) A novel dendritic cell-based cancer vaccine produces promising results in a syngenic CC-36 murine colon adenocarcinoma model. *J Surg Res* 139(2):164–169.
48. Bolesta E, et al. (2005) DNA vaccine expressing the mimotope of GD2 ganglioside induces protective GD2 cross-reactive antibody responses. *Cancer Res* 65(8):3410–3418.
49. Wierzbicki A, et al. (2008) Immunization with a mimotope of GD2 ganglioside induces CD8+ T cells that recognize cell adhesion molecules on tumor cells. *J Immunol* 181(9): 6644–6653.
50. Gil M, et al. (2009) Targeting a mimotope vaccine to activating Fcgamma receptors empowers dendritic cells to prime specific CD8+ T cell responses in tumor-bearing mice. *J Immunol* 183(10):6808–6818.
51. Mastrangelo MJ, et al. (1999) Intratumoral recombinant GM-CSF-encoding virus as gene therapy in patients with cutaneous melanoma. *Cancer Gene Ther* 6(5):409–422.
52. Shaked Y, Kerbel RS (2007) Antiangiogenic strategies on defense: On the possibility of blocking rebounds by the tumor vasculature after chemotherapy. *Cancer Res* 67(15):7055–7058.
53. Yan HH, et al. (2010) Gr-1+CD11b+ myeloid cells tip the balance of immune protection to tumor promotion in the premetastatic lung. *Cancer Res* 70(15):6139–6149.
54. Liang Z, et al. (2005) Silencing of CXCR4 blocks breast cancer metastasis. *Cancer Res* 65(3):967–971.
55. Smith MC, et al. (2004) CXCR4 regulates growth of both primary and metastatic breast cancer. *Cancer Res* 64(23):8604–8612.
56. Ravetch JV (2002) A full complement of receptors in immune complex diseases. *J Clin Invest* 110(12):1759–1761.
57. Nimmerjahn F, Ravetch JV (2005) Divergent immunoglobulin G subclass activity through selective Fc receptor binding. *Science* 310(5753):1510–1512.
58. Ravetch JV, Bolland S (2001) IgG Fc receptors. *Annu Rev Immunol* 19:275–290.
59. Nelissen JM, Peters IM, de Grooth BG, van Kooyk Y, Figdor CG (2000) Dynamic regulation of activated leukocyte cell adhesion molecule-mediated homotypic cell adhesion through the actin cytoskeleton. *Mol Biol Cell* 11(6):2057–2068.
60. van Kempen LC, et al. (2000) Activated leukocyte cell adhesion molecule/CD166, a marker of tumor progression in primary malignant melanoma of the skin. *Am J Pathol* 156(3):769–774.
61. Ihnen M, et al. (2008) Predictive impact of activated leukocyte cell adhesion molecule (ALCAM/CD166) in breast cancer. *Breast Cancer Res Treat* 112(3):419–427.
62. Prud'homme GJ, et al. (2010) Breast cancer stem-like cells are inhibited by a non-toxic aryl hydrocarbon receptor agonist. *PLoS ONE* 5(11):e13831.
63. Schneider-Gädicke A, Schwarz E (1986) Different human cervical carcinoma cell lines show similar transcription patterns of human papillomavirus type 18 early genes. *EMBO J* 5(9):2285–2292.
64. Jensen FC, Girardi AJ, Gilden RV, Koprowski H (1964) Infection of human and simian tissue cultures with Rous sarcoma virus. *Proc Natl Acad Sci USA* 52:53–59.
65. Buller RM, Chakrabarti S, Cooper JA, Twardzik DR, Moss B (1988) Deletion of the vaccinia virus growth factor gene reduces virus virulence. *J Virol* 62(3):866–874.
66. McCart JA, et al. (2001) Systemic cancer therapy with a tumor-selective vaccinia virus mutant lacking thymidine kinase and vaccinia growth factor genes. *Cancer Res* 61(24): 8751–8757.
67. Chakrabarti S, Sisler JR, Moss B (1997) Compact, synthetic, vaccinia virus early/late promoter for protein expression. *Biotechniques* 23(6):1094–1097.
68. Bradford MM (1976) A rapid and sensitive method for the quantitation of microgram quantities of protein utilizing the principle of protein-dye binding. *Anal Biochem* 72:248–254.